to positive (for 6, γ is already positive where $\mu\beta$ exhibits a negative peak; the deviation here may be, at least in part, attributable to the fact that we are comparing $\mu\beta$ with γ, as noted above).

The theoretical study provides strong evidence that, as a function of **F**, α, β, and γ are related by derivatives. Because the BOA is also determined by **F**, we can relate the derivatives back to chemical structure. In order for these derivative relations to hold in the experiments described above, it is necessary to treat donor-acceptor strength, topology, and solvent stabilization as analogous to application of an effective electric field across a conjugated π-system. Thus, of fundamental importance to our basic understanding of the structure of molecules, the derivative relations demonstrated here provide strong support for the validity of this "effective electric field" concept, as applied to linear polymethine dyes. Still an open question is how well the "effective electric field" approximation and therefore the derivative relations will apply to two-dimensional molecules or to molecules with more extended conjugation. In addition, we demonstrated, contrary to some previous assessments (*27*), that γ will be roughly zero when β is optimized. The existence of molecules with negative γ, measured well below the three-photon resonance frequency (a phenomenon that has been a subject of controversy in the nonlinear optics community) is a natural outcome of α peaking at zero BOA (a result that can be derived from simple free electron calculations) because $\partial^2\alpha/\partial\mathbf{F}^2$ is clearly negative at this point. Furthermore, predictions were made for δ as a function of molecular structure (BOA or BLA).

These results thus provide a unified picture of linear and nonlinear optical properties of linear conjugated molecules that were heretofore often treated separately. We believe that our understanding of the relation between molecular structure and β and γ has progressed to the point where the measurements of these hyperpolarizabilities can themselves be used to provide detailed insight into the chemical structure (in particular, regarding mixing of various charge-transfer resonance forms) of linear polymethine molecules.

REFERENCES AND NOTES

1. S. Dähne, *Science* **199**, 1163 (1978).
2. J. Fabian and H. Hartmann, in *Light Absorption by Organic Colorants*, K. Hafner, Ed. (Reactivity and Structure Concepts in Organic Chemistry Series, Springer-Verlag, Berlin, 1980), vol. 12.
3. J. Griffiths, *Color and Constitution of Organic Molecules* (Academic Press, London, 1976).
4. K. C. Rustagi and J. Ducuing, *Opt. Commun.* **10**, 258 (1974).
5. J. L. Oudar and D. S. Chemla, *J. Chem. Phys.* **66**, 2664 (1977).
6. ———, *Opt. Commun.* **13**, 164 (1975).
7. P. N. Prasad and D. J. Williams, *Introduction to Nonlinear Optical Effects in Molecules and Polymers* (Wiley, New York, 1991).
8. S. R. Marder, J. E. Sohn, G. D. Stucky, Eds., *Materials for Nonlinear Optics: Chemical Perspectives* (American Chemical Society, Washington, DC, 1991), vol. 455.
9. J.-L. Brédas, C. Adant, P. Tackx, A. Persoons, B. M. Pierce, *Chem. Rev.* **94**, 243 (1994).
10. S. R. Marder, D. N. Beratan, L.-T. Cheng, *Science* **252**, 103 (1991).
11. S. R. Marder *et al.*, *ibid.* **261**, 186 (1993).
12. G. Bourhill *et al.*, *J. Am. Chem. Soc.* **116**, 2619 (1994).
13. A. F. Garito, J. R. Heflin, K. Y. Wong, O. Zamani-Khamiri, in *Organic Materials for Non-linear Optics: Royal Society of Chemistry Special Publication No. 69*, R. A. Hann and D. Bloor, Eds. (Royal Society of Chemistry, Burlington House, London, 1989), pp. 16–27.
14. M. G. Kuzyk and C. W. Dirk, *Phys. Rev. A* **41**, 5098 (1990).
15. B. M. Pierce, *Proc. SPIE* **1560**, 148 (1991).
16. C. B. Gorman and S. R. Marder, *Proc. Natl. Acad. Sci. U.S.A.* **90**, 11297 (1993).
17. L. Salem, *The Molecular Orbital Theory of Conjugated Systems* (Benjamin, New York, 1966).
18. F. Meyers, S. R. Marder, B. M. Pierce, J.-L. Brédas, in preparation.
19. D. Lu, G. Chen, W. A. Goddard III, J. W. Perry, in preparation.
20. A. D. Buckingham, *Adv. Chem. Phys.* **12**, 107 (1967).
21. B. J. Orr and J. F. Ward, *Mol. Phys.* **20**, 513 (1971).
22. G. Bourhill *et al.*, *Proc. SPIE* **1853**, 208 (1993).
23. J. L. Oudar and H. L. Person, *Opt. Commun.* **15**, 258 (1975).
24. B. F. Levine and C. G. Bethea, *Appl. Phys. Lett.* **24**, 445 (1974).
25. K. D. Singer and A. F. Garito, *J. Chem. Phys.* **75**, 3572 (1981).
26. L.-T. Cheng *et al.*, *J. Phys. Chem.* **95**, 10631 (1991).
27. C. W. Dirk, L.-T. Cheng, M. Kuzyk, *Int. J. Quant. Chem.* **43**, 27 (1992).
28. C. Reichardt, *Solvents and Solvent Effects in Organic Chemistry* (VCH, Weinheim, Germany, ed. 2, 1988).

29. The research described in this report was performed in part by the Jet Propulsion Laboratory (JPL), California Institute of Technology, as part of its Center for Space Microelectronics Technology and was supported by the Advanced Research Projects Agency (administered by the Air Force Office of Scientific Research) and the Ballistic Missiles Defense Initiative Organization, Innovative Science and Technology Office, through a contract with the National Aeronautics and Space Administration (NASA). Work done at the Beckman Institute was supported by the National Science Foundation, the Air Force Office of Scientific Research, and the North Atlantic Treaty Organization. G.B. thanks the National Research Council and NASA for a Resident Research Associateship at JPL. The work in Mons is carried out within the framework of the Belgium Prime Minister Office of Science Policy "Pôle d'Attraction Interuniversitaire en Chimie Supramoléculaire et Catalyse" and "Programme d'Impulsion en Technologie de l'Information" and is supported in part by the Belgium National Fund for Scientific Research (FNRS). We thank K.-T. Lim, B. G. Tiemann, D. N. Beratan, and L.-T. Cheng for helpful discussions.

1 March 1994; accepted 6 June 1994

A Formation Mechanism for Catalytically Grown Helix-Shaped Graphite Nanotubes

S. Amelinckx, X. B. Zhang,* D. Bernaerts, X. F. Zhang,† V. Ivanov,‡ J. B. Nagy

The concept of a spatial-velocity hodograph is introduced to describe quantitatively the extrusion of a carbon tubule from a catalytic particle. The conditions under which a continuous tubular surface can be generated are discussed in terms of this hodograph, the shape of which determines the geometry of the initial nanotube. The model is consistent with all observed tubular shapes and explains why the formation process induces stresses that may lead to "spontaneous" plastic deformation of the tubule. This result is due to the violation of the continuity condition, that is, to the mismatch between the extrusion velocity by the catalytic particle, required to generate a continuous tubular surface, and the rate of carbon deposition.

The formation of coiled carbon fibers and their morphology have been described recently in a number of papers (*1–10*). The fibers were found to be hollow tubes consisting of concentric cylindrical graphene sheets. They are prepared by the high-temperature (600° to 700°C) catalytic decomposition of organic vapors such as acetylene or benzene on a finely divided metallic catalyst such as Co, Fe, or Ni. The tubules can adopt various shapes such as straight, curved, planar-spiral, and helix, often with a remarkably constant pitch. It is generally accepted that the tubules grow by the extrusion of carbon, dissolved in a metallic catalyst particle that is oversaturated in carbon at one part of the surface. The most detailed description of the growth process was given by Baker (*1*), who emphasized the chemical aspects and treated only the case of straight cylindrical tubes.

S. Amelinckx, X. B. Zhang, D. Bernaerts, X. F. Zhang, EMAT, University of Antwerp (RUCA), Groenenborgerlaan 171, B-2020 Antwerp, Belgium.
V. Ivanov and J. B. Nagy, ISIS, University of Namur, rue de Bruxelles 61, B-5000 Namur, Belgium.

*Permanent address: Department of Materials Science and Engineering, Zhejiang University, Hangzhou, People's Republic of China.
†Permanent address: Beijing Laboratory of Electron Microscopy, Chinese Academy of Sciences, People's Republic of China.
‡Permanent address: Chemistry Department, Moscow State University, Moscow, Russia.

So far, a consistent explanation of the growth of helix-shaped carbon nanotubules is lacking, although an attempt was made to discuss the possible role of the anisotropy of the particle surfaces (*5*).

In a recent paper, we gave a detailed description of the fabrication procedure for well-graphitized and extremely thin coiled nanotubules (the coil radius of the smallest one is about 6 nm), with cobalt as a catalyst and acetylene as the carbon source (*9*). We also studied the morphology and the internal structure of such fibers by high-resolution imaging and by electron diffraction (*10, 11*). Here, we present a detailed and coherent picture of the growth mechanism for the various observed shapes. A survey of the morphology of the graphite nanotubes of interest is given in Fig. 1. The internal structure of a helix-shaped tube is visible in Fig. 2, where the graphite spacing of 0.34 nm is imaged. The graphite texture of the catalytically grown straight tubules is the same as that of the fibers grown by electric arc (*12*). The growth mechanism must be different, however, because metallic particles do not seem to play an essential role in the electric arc process. Moreover, helix-shaped tubules have only been observed in the catalytically grown fibers.

A growth mechanism for helix-shaped tubules should be sufficiently general to account for the variability in pitch of the helices, for the occasional formation of planar spirals, and for the formation of straight tubes. Catalytic particles are involved in this mechanism (*3*) and help to determine the cross section of the tubules. The distinction between mechanisms, whereby the particle promotes "tip growth" or "base growth," does not appear to be essential because in both cases the tubule grows away from the particle by the deposition of carbon in the contact region (C) between the particle and the already formed tubule segment. We discuss growth, assuming that the ring-shaped tube nucleus has formed already. The initial tube is assumed to serve as a template for the deposition of successive layers. However, the initial tube could be multilayered already. Whether the carbon diffuses through the particle before precipitating at the surface of the particle (*1, 2, 13*) or is formed directly from the gas phase at the surface area in contact with the tubule is also not essential for the geometry of the process.

Figure 3 shows that tip and base growth probably both occur, either simultaneously or in succession. Here, the initial tubule must have been formed to a large extent from the particle that afterward became encapsulated in the tube, perhaps according to a scenario shown in Fig. 4, A to F. In the first stage, the particle is lifted by the growing tubule, with carbon deposited at the annular contact with the particle and at the bottom contact with the support. After the particle is captured within the tube, further growth may presumably be continued by the catalyst at the support.

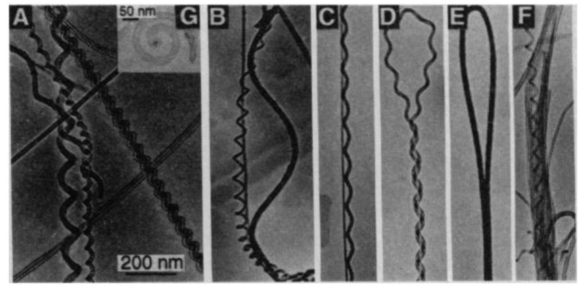

Fig. 1. Graphite tubules grown by the cobalt-catalyzed decomposition of acetylene, exhibiting various shapes. (**A**) Helix-shaped tubules having pitches of different magnitudes. Straight tubules are also present; one is single and straight, a second one is bent, and the third consists of a pair of parallel tubules kept together by Van der Waals attraction. (**B**) Complicated interaction between straight and helix-shaped tubules. (**C**) Parallel arrangement of a straight and a helix-shaped tubule, presumably kept together by Van der Waals attraction. (**D**) Coiled tubule intercoiling with itself after having made a U-turn. (**E**) Straight tubule making a closed loop, the straight ends sticking together. (**F**) Bundle of parallel straight tubules and one helix. (**G**) Planar spiral-shaped tubule.

Tip growth as well as base growth is consistent with the assumption that growth occurs by the extrusion of carbon along the contact curve between the particle and the already formed tube. In the case of the growth of a straight tube, the longitudinal growth velocity, v_l or the speed of extrusion, is the same all along the ring-shaped area (C) where carbon is being "deposited."

To describe the growth process more quantitatively, the concept of a "spatial hodograph" of the growth velocity $\mathbf{v}_l$ along the curve (C) is introduced (*14*), which ignores the atomic structure and considers the graphene sheet as a continuum. For simplicity, we first assume the curve (C) to be planar and circular. If the velocity vector $\mathbf{v}_0$ is perpendicular to the plane of (C) and is constant along the ring as in Fig. 5A, a straight tubule is formed because successive growth fronts, corresponding to successive small time intervals, are related by the parallel translation $\mathbf{v}_0$. Unfolding the cylindrical surface in a plane gives a "planar hodograph." For a straight tube, the resulting graph of v_l versus the azimuth φ is simply a straight line parallel to the φ axis. The surface area under the hodograph is a measure of the amount of material deposited per unit of time (Fig. 5B).

However, as is suggested in (*5*), the catalytic activity is often anisotropic and inhomogeneous because it depends on the exposed crystal facet of the particle and on its topography. The spatial hodograph of the extrusion speed can therefore be more complicated and may, for instance, be as it is sketched in Fig. 5, C and D. However,

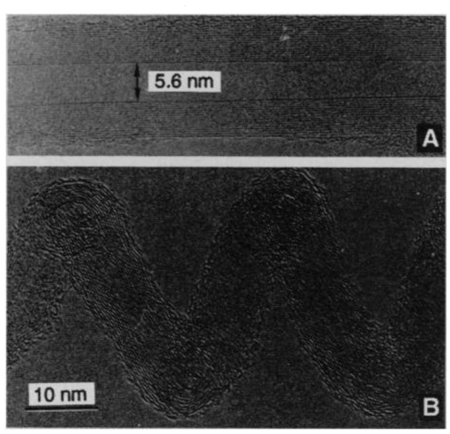

Fig. 2. High-resolution images of (**A**) a helix-shaped tubule containing 11 graphene tubes and (**B**) a straight tubule containing 17 graphene sheets. The fringe spacing is consistent with the graphite spacing, C/2 = 0.34 nm.

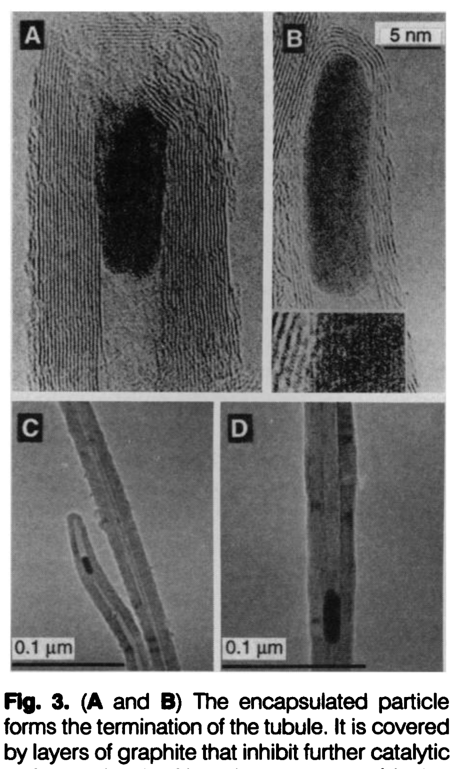

Fig. 3. (**A** and **B**) The encapsulated particle forms the termination of the tubule. It is covered by layers of graphite that inhibit further catalytic action at the tip. Note the presence of lattice fringes in the catalytic particle in (B); the inset shows it at higher magnification. (**C** and **D**) Catalytic particles encapsulated in tubules. The central channel changes in width at the level of the particle.

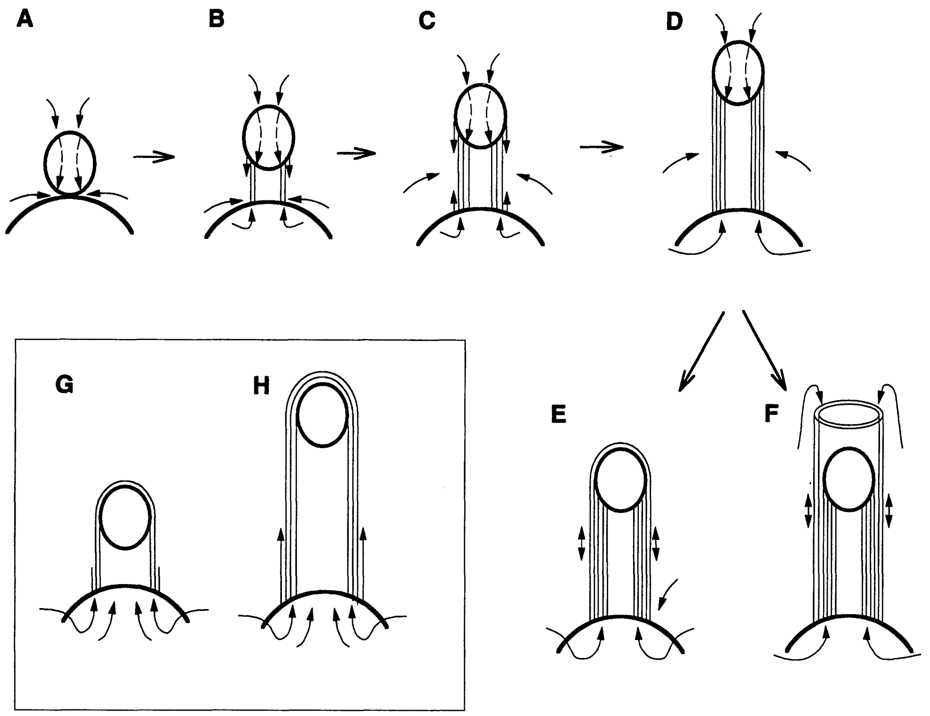

Fig. 4. Growth stadia of a nanotubule. (**A**) A small catalytic particle resting on a larger one that acts as a support. (**B** and **C**) The small particle "lifted" away from the support by the deposition of graphene sheets, formed from carbon diffusing through the small catalytic particle and through the base. (**D**) The outer diameter of the tubule becoming equal to the particle size. (**E**) A layer of graphite covering the small particle and inhibiting further tip growth of the tubule (see the observations for Fig. 3, A and B). (**F**) Tubular layers fed by the supporting particle grown beyond the small particle. Eventually the tube may become closed (see the observation for Fig. 3, C and D). (**G** and **H**) The particle already covered by a graphite layer during the initial stage. Further growth occurs by extrusion through the base, and diffusion occurs along the graphite surface.

the continuity of the tube imposes the condition that the loci of points reached at successive instants be related to the curve (C) by translations, rotations, or both. If this were not the case, the integrity of the tube would not be maintained. This continuity condition restricts the possible shapes of hodographs; in particular, it requires that the endpoints of all vectors be situated in a plane. One has thus to distinguish between the particle hodograph representing the catalytic activity along (C) and the growth hodograph representing the speed of propagation of the growth front, which is subject to the condition just mentioned. In a real growth process, the two have to be matched by the formation of a tubular surface of the adequate geometry. If perfectly matched, the resulting tubular surface will be "stress-free." By this term we mean free of stresses other than those arising from its curved shape. If the two do not match, additional growth-induced stresses will arise, as discussed below.

The simplest non-trivial hodograph leading to a curved tubule and in which the velocity vectors are normal to the plane of (C) is shown in Fig. 6. The endpoints of $\mathbf{v}_l$ terminate in a plane that is not parallel to the plane of (C). The spatial hodograph is represented in Fig. 6A, and the corresponding planar hodograph is represented in Fig. 6B. The latter is a sinusoid with a maximum velocity v_M, and a minimum velocity, v_m, corresponding to diametrically opposed points of (C); it is symmetric with respect to the minimum .and the maximum. Growth based on such a hodograph causes curvature of the tubule (see Fig. 6, E to G, where the time increment Δt is arbitrarily small), the axis of curvature being the intersection line of the planes Π_1 and Π_0 (Fig. 6A). The resulting tube will be a torus, the radius, R_0, of which is given by

$$R_0 = r(v_M + v_m)/(v_M - v_m) = 2rv_c/\Delta v \quad (1)$$

where r is the radius of the tube, which is directly related to the size of the catalytic particle, and $v_c = (1/2)(v_M + v_m)$. The point b generates the outer rim, and a generates the inner rim of the torus. If $\Delta v = v_M - v_m$ decreases or increases in the course of time, the tubule becomes a planar spiral (Fig. 1G). A completely closed torus cannot be formed, but tubules such as the one shown in Fig. 1E have grown in their curved part according to such a hodograph with variable Δv.

Generally, curve (C) may deviate from a circle (for instance, be ellipse-shaped as in Fig. 7). However, the stable cross section of a graphene tube is circular. For this shape, the strain energy associated with formation of the cylindrical surface out of a planar sheet is a minimum. The strain energy is then uniformly distributed along the whole surface, the curvature being the same along the cross section (*13*). A tube formed from an ellipse-shaped curve (C) will therefore tend to become circular. This theoretical argument is consistent with the observation that all helix-shaped tubes studied in cross section were found to be roughly circular. Because it is probable that the ring-shaped nuclei have a variety of initial shapes, deviating more or less from the circular, the observed circular cross sections can be rationalized most simply by assuming that the tubes grow along a direction inclined with respect to the plane Π_0 of (C) so as to approximate a circular cross section. The spatial hodograph is then as it is shown in Fig. 7A; the corresponding planar hodograph is clearly equivalent to that of Fig. 5B.

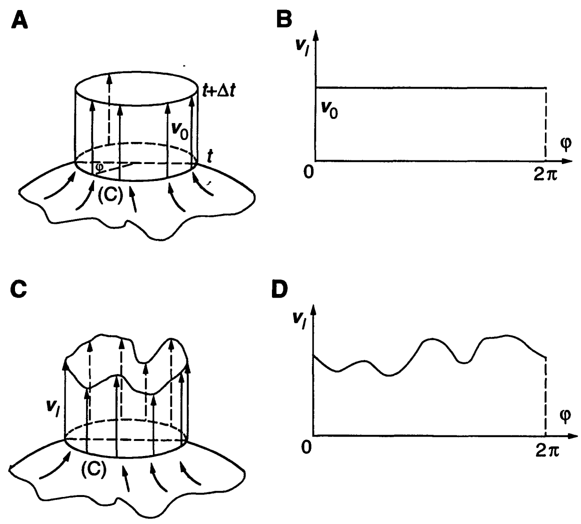

Fig. 5. Hodograph of the extrusion velocities for the formation of straight tubules. The locus of active sites is a circle (C). (**A**) Spatial hodograph: The extrusion velocity is constant along (C). (**B**) Planar hodograph corresponding to (A): The surface area under the hodograph is proportional to the amount of extruded material. (**C**) General spatial hodograph. (**D**) Planar hodograph corresponding to (C).

A straight tube is formed along a direction inclined with respect to (C). Note that the tubular surface can be formed by the translation along vector $\mathbf{v}_0$ of the curve (C).

To generate a helix-shaped tube, the hodograph must be a combination of a hodograph of the type shown in Fig. 7A and of that represented in Fig. 6A. Such a spatial hodograph is shown in Fig. 7B. The line l is the intersection of Π_1 and Π_0. The continuity condition is satisfied because all velocity vectors terminate in a plane. The difference of the components of v_m and v_M normal to this intersection line causes a rotation of (C) and so leads to wrapping of the tube on a cylinder while the inclusion angle, α, causes a translation and determines the pitch, along with v_c and Δv.

As shown below (*15*), the geometrical parameters of the resulting helix can be deduced from the model and expressed in terms of the extreme values v_M and v_m of the extrusion velocity and of the inclination angle. The difference in velocity, Δv, causes the plane of the growth front to rotate about l (Fig. 7B) with an angular velocity given by

$$\omega = d\beta/dt = \Delta v \sin \alpha/2r \qquad (2)$$

The time needed to form one complete spire of the helix described by the point c is thus

$$t = 4\pi r/\Delta v \sin \alpha \qquad (3)$$

The radius R_0 of this helix is given by Eq. 1, and its pitch is given by

$$p = 4\pi r(v_c/\Delta v) \operatorname{cotan} \alpha \qquad (4)$$

The special configuration of Fig. 7 was selected because it could be conveniently represented. The limiting plane Π_1 of the hodograph was chosen in such a way that the intersection line, l, of Π_0 and Π_1 is parallel to the projection of v_c on Π_0. For a general orientation of Π_1, the intersection line encloses an angle γ with the projection of v_c on Π_0. In that case, Eqs. 1 and 2 must be adapted. Now $R_0 = 2rv_c/\Delta v \cos \gamma$, but because $\omega = \Delta v \sin \alpha \cos \gamma/2r$, Eq. 4 for the pitch remains unchanged.

The proposed mechanism gives rise to the formation of a stress-free tubular surface, provided the continuity condition for the extrusion velocities is obeyed. However, the catalytic activity of the particle in general does not obey this condition. Its planar hodograph may, for instance, be as shown by a thin line in Fig. 6B for the simplest nontrivial case of the torus. The full line then represents the closest approximation to the real hodograph describing the displacement rate of the growth fronts by means of a sinusoid, which would satisfy the continuity condition. The initial mismatch between the two hodographs tends to disappear, and a stationary regime is established whereby any initial difference is minimized and a smooth profile that approximately satisfies the continuity condition is realized. At the points where excess carbon is generated the resulting compressive stress slows the carbon deposition rate, and in points where too little carbon is produced the resulting tensile stress tends to increase the deposition rate of carbon. This feedback process is responsible for the stationary regime and leads to a compromise that may correspond to a spatial hodograph not satisfying the continuity condition, thus leading to a stressed situation. The shaded areas in Fig. 6B correspond to the deposition of an excess (+) or a deficiency (−) of carbon, as compared to the quantity needed to form a stress-free tube. The figure shows that in areas 1 and 4 of the torus too much material is deposited, whereas in areas 2 and 3 not enough material is deposited. This difference causes the inner rim of the torus to be under compressive stress while the outer rim is under traction, with the dotted line representing a neutral surface along which the stress changes sign (Fig. 6, C and D). Because graphite is strong in tension and because of the absence of shear stresses, the outer rim of the torus may only be elastically deformed. However, large stresses may induce the formation of pentagonal meshes in the graphite network to relieve part of the stresses. Such pentagonal meshes, which cause positive curvature (elliptic points), are present at +60° disclina-

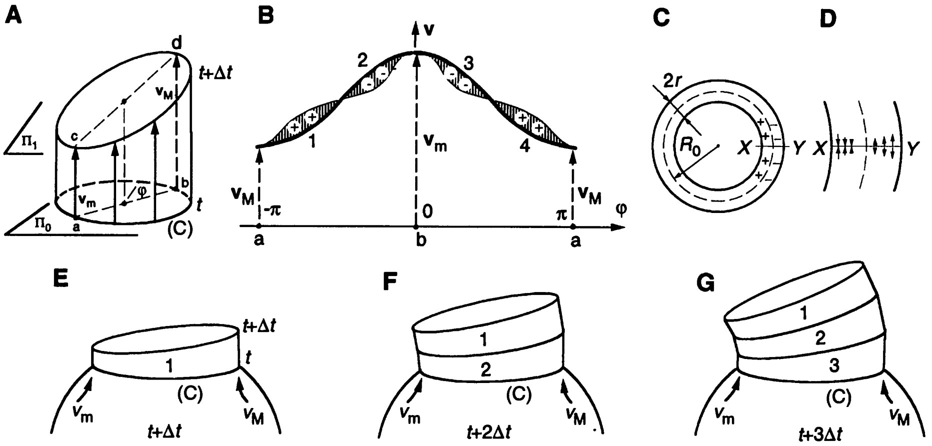

Fig. 6. (**A** and **B**) Hodograph of the extrusion velocities for the case of a uniformly bent tubule. The active sites are on a circle (C). (A) Spatial hodograph: The locus of the endpoints of the velocity vectors is a planar curve in an inclined plane. The point a generates the inner rim of the torus, and b generates the outer rim. (B) Planar hodograph. The full line is a sinusoid obeying the continuity condition for the growth of a uniformly bent tubule. The thin line represents the hodograph of the extrusion velocity. Note the mismatch between the two curves. The cross-hatched areas correspond to an excess (+) or a deficiency (−) of carbon. Stress distribution in a torus formed according to the dotted hodograph of (B). (**C** and **D**) The outer rim is under tensile stress, and the inner rim is under compressive stress. For (C), the excess and deficiency regions are indicated. For the stress distribution in (D), the dotted line is the neutral surface. (**E** to **G**) Successive stages in the extrusion of carbon according to the hodograph in (A). The resulting tubule is a torus and has a constant curvature. The time interval, Δt, is arbitrarily small.

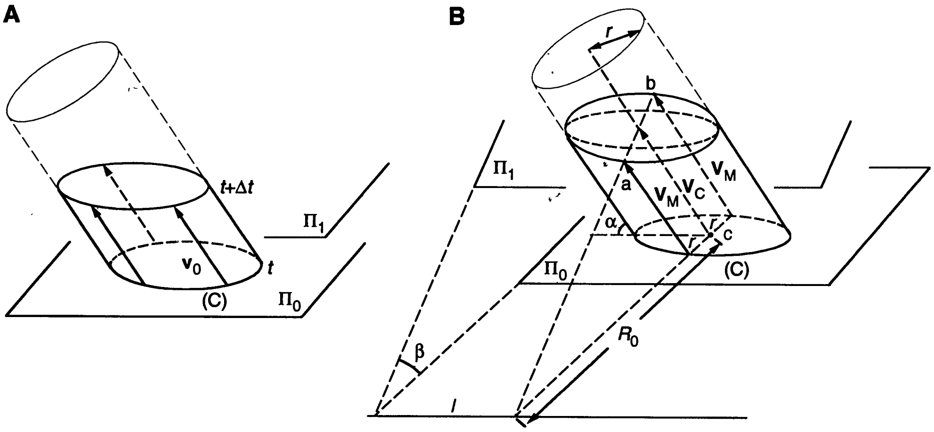

Fig. 7. (**A**) Hodograph of a straight tubule. The locus of active sites is an ellipse. Because the tube is a circular cylinder, it must be inclined with respect to Π_0. (**B**) Spatial hodograph generating a helix-shaped tube. The locus of the endpoints of the velocity vectors is a planar curve in Π_1 that is inclined with respect to Π_0. The velocity vectors form an angle α with Π_0.

tions, that is, they are associated with the removal of a 60° wedge from the hexagonal network (*12, 16, 17*). On the other hand, graphite deforms by "kinking" when it is under compressive stresses parallel to the basal planes. In general, the growth-induced stresses seem to be sufficiently large to activate this mode of plastic deformation, as shown in some of the illustrated tubules in (*11*). However, part of the compressive stresses may also be relieved by the formation of heptagons associated with −60° disclinations, that is, with the insertion of a 60° wedge that causes negative curvature (hyperbolic points). The occurrence of pentagon-heptagon pairs minimizes the long-range stresses. These considerations may readily be extended to helices. They explain why most of the graphite helices show deformation patterns, which are characteristic of kinking, preferentially along the inner rim (*11*), or polygonization suggestive of the presence of (5-7) ring pairs as discussed in (*10*).

The mobility of a particle promoting tip growth is appreciable, because the particle rests on a film of carbon atoms that has fluid-like characteristics (*3*). If the spatial hodograph of the particle is asymmetric with respect to the line cd (Fig. 6A), the continuity condition cannot be satisfied. The planar hodograph is then asymmetrical as well. More material tends to be deposited on one side of the symmetry line cd than on the other side. This difference causes the particle to be tilted about the line cd, thereby changing the azimuth of the line connecting the minimum and maximum in the spatial hodograph. Tilting of the particle may thus lead to a change in azimuth of the hodograph, which in turn changes the bending axis of the tubular surface. One can thus envisage that under rather special conditions the particle describes a precession motion, imposing a continuous rotation in the azimuth of the hodograph. This rotation would lead to the formation of a coiled tube wound on a toroidal surface rather than on a cylinder. An example of a tubule that was presumably formed partly in this manner is shown in Fig. 1D.

Because the catalytic activity of a particle may change in the course of time due to local poisoning, for example, the hodograph is often time-dependent. The resulting tubular surfaces may then have complicated shapes such as a helix with a variable pitch. However, the radius of the tubule remains roughly constant because this parameter depends mainly on the size of the active particle. The growth-induced stresses may further lead to complicated deformation patterns of the tubules that may in part account for the observed polygonization of helices (*10, 11*). The stresses could be periodically relieved by the introduction of (5-7) ring pairs when the elastic limit is exceeded.

REFERENCES AND NOTES

1. R. T. K. Baker, *Carbon* **27**, 315 (1989).
2. ———, P. S. Harris, S. Terry, *Nature* **253**, 37 (1975); R. T. K. Baker and J. J. Chludzinski, *J. Catal.* **64**, 464 (1980).
3. A. Oberlin, M. Endo, T. Koyama, *J. Cryst. Growth* **32**, 335 (1976).
4. R. E. Smalley, "Regulation of Proteins by Ligands," Proceedings of the Robert A. Welch Foundation Conference on Chemical Research XXXVI, Houston, TX, 26 to 27 October 1992, p. 161.
5. S. Motojima, M. Kawaguchi, K. Nozaki, H. Iwanaga, *Carbon* **29**, 379 (1991); S. Motojima, J. Hasegawa, M. Kawaguchi, K. Nozaki, H. Iwanaga, *J. Chem. Vapor Deposition* **1**, 137 (1992).
6. M. José-Yacaman, M. Miki-Yoshida, L. Rendon, J. G. Santiesteban, *Appl. Phys. Lett.* **62**, 657 (1993).
7. D. S. Bethune *et al.*, *Nature* **363**, 605 (1993).
8. N. M. Rodriguez, *J. Mater. Res.* **8**, 3233 (1993).
9. V. Ivanov *et al.*, *Chem. Phys. Lett.*, in press.
10. X. B. Zhang *et al.*, *Europhys. Lett.*, in press.
11. D. Bernaerts *et al.*, unpublished results.
12. S. Iijima, T. Ichihashi, Y. Ando, *Nature* **356**, 776 (1992).
13. G. G. Tibbets, *J. Cryst. Growth* **66**, 632 (1984).
14. A hodograph is a geometrical locus of the endpoints of the vectors describing the extrusion velocity (or the growth velocity) in the points along a curve.
15. From Fig. 7B follows (i) $tg\beta = t\Delta v \sin\alpha/2r$ or (ii) by differentiation, $d\beta/\cos^2\beta = (\Delta v \sin\alpha/2r)dt$, because $t\Delta v << r$; for sufficiently small t this expression leads with a good approximation to Eq. 2, and $t = 2\pi/\omega$ leads to Eq. 3. With the radius $R_0 = v_c \sin\alpha(dt/d\beta)$ or with Eq. 2 and (ii), Eq. 1 follows. The pitch p is the lateral displacement parallel to l of the point c after a complete turn (or a period t); hence, $p = tv_c\cos\alpha$ (iii), or using Eq. 3 one finds Eq. 4. The observed values of r, α, p, and R_0, which are related by $\cot\alpha = p/2\pi R_0$, lead to $\Delta v/v_c = 0.08$ for the tubule shown in Fig. 2.
16. M. Kléman, in *Dislocations in Solids*, F. R. N. Nabarro, Ed. (North-Holland, Amsterdam, 1980), vol. 5, p. 350.
17. J. Friedel, *Dislocations* (Pergamon, Oxford, 1964).

18. We thank D. Van Dyck, G. Van Tendeloo, J. Van Landuyt, A. Lucas, and P. Lambin for useful discussions and for their continued interest in this research. Supported in part by the Belgian National Program of Inter-University Research Projects initiated by the State Prime Minister Office (Science Policy Programming) and by the Regional Government of Wallonie for a project on Fullerenes. The members of the EMAT and ISIS laboratories also acknowledge the National Fund for Scientific Research.

4 April 1994; accepted 6 June 1994

A Devonian Tetrapod from North America

Edward B. Daeschler,* Neil H. Shubin, Keith S. Thomson, William W. Amaral

An early tetrapod fossil from the Upper Devonian of Pennsylvania (Catskill Formation) extends the temporal range of tetrapods in North America and suggests that they attained a virtually global equatorial distribution by the end of the Devonian. Derived features of the shoulder girdle indicate that appendicular mechanisms of support and propulsion were well developed even in the earliest phases of tetrapod history. The specialized morphology of the pectoral skeleton implies that the diversity of early tetrapods was great and is suggestive of innovative locomotor patterns in the first tetrapods.

The origin of terrestrial vertebrates is one of the major events in the history of animal life. The transition from life in water to life on land was extremely complex. Current controversy centers on the evolutionary relations between fish and tetrapods, the timing of tetrapod origins, the early biogeographic history of tetrapods, and the functional and physiological changes that allowed the invasion of terrestrial ecosystems (*1, 2*). Fossil evidence of the earliest tetrapods comes from a small number of widely scattered Upper Devonian localities [~370 to 362 million years ago (Ma)]. The most complete material consists of partially articulated skeletons of *Ichthyostega* and *Acanthostega* from East Greenland (*3*). Less completely preserved remains of other Upper Devonian tetrapods have been recovered from sites in Scotland (*4*), Latvia (*5*), Russia (*6*), and Australia (*7*). Devonian tetrapod trackways, which are much less reliable evidence, have been reported from Australia (*8*) and Brazil (*9*). Here we describe an Upper Devonian tetrapod from continental North America. The specimens include early, well-preserved shoulder girdles that provide an understanding of forelimb function during the early diversification of tetrapods.

Hynerpeton bassetti gen. nov. sp. nov. (*10*) was collected in 1993 near the village of Hyner in Clinton County, Pennsylvania, USA. The specimens (*11*) are from the Duncannon Member (*12*) of the Catskill Formation. They are Middle to Upper Famennian in age (Late Devonian, ~365 to 363 Ma).

E. B. Daeschler, Academy of Natural Sciences of Philadelphia, 1900 Benjamin Franklin Parkway, Philadelphia, PA 19103–1195 and Department of Geology, University of Pennsylvania, Philadelphia, PA 19104–6316, USA.
N. H. Shubin, Department of Biology, University of Pennsylvania, Philadelphia, PA 19104–6017, USA.
K. S. Thomson, Academy of Natural Sciences of Philadelphia, 1900 Benjamin Franklin Parkway, Philadelphia, PA 19103–1195, USA.
W. W. Amaral, Museum of Comparative Zoology, Harvard University, Cambridge, MA 02138, USA.
*To whom correspondence should be addressed.